

# Dodecin Is the Key Player in Flavin Homeostasis of Archaea<sup>5</sup>

Received for publication, October 21, 2008, and in revised form, January 9, 2009. Published, JBC Papers in Press, February 17, 2009, DOI 10.1074/jbc.M808063200

Martin Grninger<sup>†1</sup>, Heike Staudt<sup>§</sup>, Patrik Johansson<sup>‡</sup>, Josef Wachtveitl<sup>§</sup>, and Dieter Oesterhelt<sup>†2</sup>

From the <sup>†</sup>Department of Membrane Biochemistry, Max Planck Institute of Biochemistry, Am Klopferspitz 18, 82152 Martinsried and the <sup>§</sup>Institute of Physical and Theoretical Chemistry, Goethe University Frankfurt am Main, Max-von-Laue-Strasse 7, 60438 Frankfurt am Main, Germany

Flavins are employed to transform physical input into biological output signals. In this function, flavins catalyze a variety of light-induced reactions and redox processes. However, nature also provides flavoproteins with the ability to uncouple the mediation of signals. Such proteins are the riboflavin-binding proteins (RfBPs) with their function to store riboflavin for fast delivery of FMN and FAD. Here we present *in vitro* and *in vivo* data showing that the recently discovered archaeal dodecin is an RfBP, and we reveal that riboflavin storage is not restricted to eukaryotes. However, the function of the prokaryotic RfBP dodecin seems to be adapted to the requirement of a unicellular organism. While in eukaryotes RfBPs are involved in trafficking riboflavin, and dodecin is responsible for the flavin homeostasis of the cell. Although only 68 amino acids in length, dodecin is of high functional versatility in neutralizing riboflavin to protect the cellular environment from uncontrolled flavin reactivity. Besides the predominant ultrafast quenching of excited states, dodecin prevents light-induced riboflavin reactivity by the selective degradation of riboflavin to lumichrome. Coordinated with the high affinity for lumichrome, the directed degradation reaction is neutral to the cellular environment and provides an alternative pathway for suppressing uncontrolled riboflavin reactivity. Intriguingly, the different structural and functional properties of a homologous bacterial dodecin suggest that dodecin has different roles in different kingdoms of life.

Flavins are a major class of cofactors that are able to accept and donate electrons as well as to absorb visible light. Flavins consist of a nonconserved aliphatic moiety, covalently linked to a conserved aromatic isoalloxazine ring (Fig. 1 and supplemental Fig. 1). The distribution of flavins in nature correlates with the complexity of the aliphatic chain. Although FMN (phosphoribityl chain) and FAD (ADP-ribityl) are widespread among flavoenzymes, a function of riboflavin (RF,<sup>3</sup> ribityl) as a catalyt-

ically active compound has not been reported to date (1); instead, RF acts as the direct precursor for FMN and FAD in flavin biosynthesis.

In all flavins, the catalytically active unit is the isoalloxazine substructure (2–4). To handle the reactivity of the isoalloxazine ring, FMN and FAD are tightly bound to flavoenzymes. Finely tuned binding restricts the reaction spectrum of FMN and FAD to discrete, beneficial reaction pathways, preventing harmful side reactions. Reported functions of flavoenzymes include transferring electrons from and to reactive centers (e.g. respiratory chain) as well as employing light for the induction of radical reactions (e.g. DNA-photolyase) or conformational changes (e.g. phototropin) (5–8). In the biosynthesis, the full catalytic power of flavins has already formed at the stage of the FMN and FAD precursor RF (see Fig. 1). As RF is not used as an enzymatically active compound, it is, different to FMN and FAD, not integrated into flavoenzymes. To avoid a negative impact of uncontrolled flavin reactivity by free RF, nature established sequestering devices termed riboflavin-binding proteins (RfBPs). These proteins have been shown to store and distribute RF in eukaryotes, ensuring a fast supply of FMN and FAD (9, 10).

The small flavoprotein dodecin from the archaeon *Halobacterium salinarum* was reported to bind RF with high affinity and to extensively quench flavin fluorescence, thus exerting the key functions of RfBPs (11). Additional affinity for lumichrome (LCR) could moreover characterize dodecin as a protein with a dual binding mode (12–14). Based on sequence conservation, dodecins cluster in an archaeal and a bacterial subgroup. The majority of dodecins occur in bacteria, some among pathogenic organisms such as *Mycobacterium tuberculosis* or *Pseudomonas aeruginosa*. Here we present data that identify dodecin from *H. salinarum* as an RfBP. By storing RF in micromolar amounts during growth-limiting conditions, and providing it for the biosynthesis of FMN and FAD at high metabolic activities, the archaeal dodecin acts as an RF buffer, balancing the total flavin concentration during the *H. salinarum* life cycle. Analysis of the 40% sequence-identical bacterial dodecin from *H. halophila* reveals different structural and functional properties and excludes an RF binding and storing function. Although the archaeal dodecin represents the first RfBP described in prokaryotes, the role of the bacterial dodecin remains speculative.

## EXPERIMENTAL PROCEDURES

*Preparation of Vectors and Strains and Purification of Proteins*—Cloning, purification, refolding, and reconstitution of proteins HhDod<sup>B</sup>, HsDod<sup>A</sup>, and HsDod<sup>A;E45A</sup> were performed as described earlier (13). *H. salinarum* strains R1Δdod

<sup>5</sup> The on-line version of this article (available at <http://www.jbc.org>) contains additional Experimental Procedures, Figs. 1–8, Tables 1–3, and additional references.

The atomic coordinates and structure factors (codes 2vxa and 2vx9) have been deposited in the Protein Data Bank, Research Collaboratory for Structural Bioinformatics, Rutgers University, New Brunswick, NJ (<http://www.rcsb.org/>).

<sup>1</sup> To whom correspondence may be addressed. Tel.: 49-89-8578-2382; Fax: 49-89-8578-3557; E-mail: gringing@biochem.mpg.de.

<sup>2</sup> To whom correspondence may be addressed. Tel.: 49-89-8578-2386; Fax: 49-89-8578-3557; E-mail: oesterhe@biochem.mpg.de.

<sup>3</sup> The abbreviations used are: RF, riboflavin; RfBP, riboflavin-binding protein; HsDod, archaeal *H. salinarum* dodecin (ligand composition not specified); HhDod, bacterial *H. halophila* dodecin (ligand composition not specified); LCR, lumichrome; RT, real time; TdDod, bacterial *T. thermophilus* dodecin.

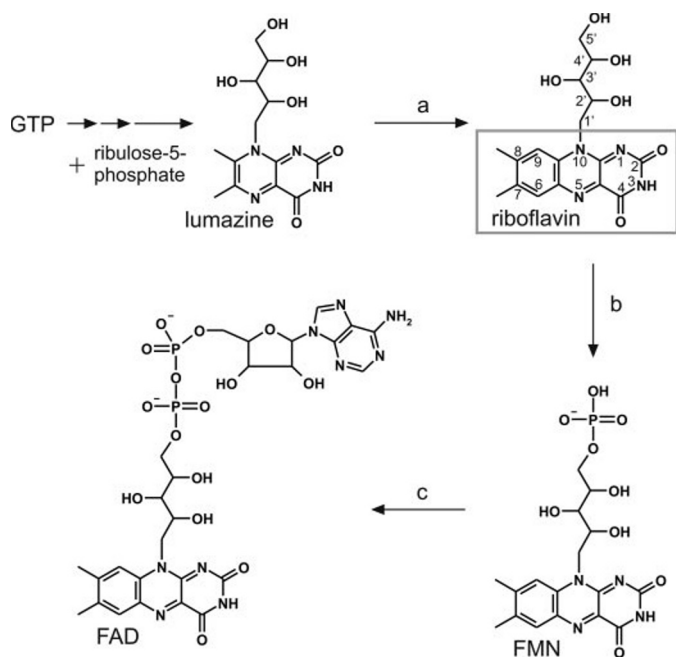


FIGURE 1. **Flavin biosynthesis.** GTP and ribulose 5-phosphate are the educts in flavin synthesis. The key step in flavin biosynthesis is the dismutase reaction catalyzed by riboflavin synthase (a), building the tricyclic heteronuclear organic ring isoalloxazine. RF is further converted into FMN by riboflavin kinase (b) and subsequently transformed into FAD by FAD synthase (c). The catalytically active isoalloxazine is highlighted by a gray rectangle in the RF chemical structure. For a more detailed description of the flavin biosynthesis see supplemental Fig. 1.

and R1dodHis<sup>+</sup> are derivatives of the *H. salinarum* strain R1 (DSM 671) and were generated by a blue-red selection strategy, based on the PMKK100 vector (15), and on the base of the pBPH-M vector, respectively (16).

**Light Stability of Riboflavin and Spectroscopic Characterization**—For the determination of RF stability, free and dodecin-bound RF were illuminated with a high pressure mercury lamp at 800 milliwatt/cm<sup>2</sup> radiation energy. A 3-mm KG1 filter was used to absorb light of short (<300 nm) and long (>700 nm) wavelength from the light source. The decomposition was monitored with absorption spectroscopy and fluorescence detection of chromatographically separated samples. Oxygen-free conditions were achieved by several cycles of degassing the reaction solution under argon atmosphere. Femtosecond pump/probe experiments were performed as described elsewhere (17).

**Western Blotting and RT-PCR**—For determination of the dodecin expression profile, samples of lysates (volumes of samples related to the optical density of the cell culture) were separated using SDS-PAGE and immobilized on polyvinylidene difluoride membranes. Dodecin was detected using polyclonal IgY anti-dodecin antibodies. RT-PCR was performed as described elsewhere (18).

**Quantitative Analysis of Riboflavin and Lumichrome**—For analysis of the intracellular flavin concentrations, a cell lysate of *H. salinarum* was treated with ethanol at 80 °C. After centrifugation, the supernatant was chromatographically separated on a reversed phase column, and flavins were monitored by simultaneous detection at wavelength couples 381/464 and 450/520 nm. For analysis of LCR, a sample of the lysate was additionally

treated with acetonitrile. Nickel-chelating chromatography was used for determination of ligands bound to His-tagged dodecin.

**Crystallization of HhDod<sup>B</sup> and HsDod<sup>A;E45A</sup>**—Diffracting crystals of HhDod<sup>B</sup> grew in 0.4 M NH<sub>4</sub>H<sub>2</sub>PO<sub>4</sub> and 0.1 M ectoin at 18 °C by the vapor diffusion technique. HsDod<sup>A;E45A</sup> was crystallized under identical conditions as HsDod<sup>A</sup> (13). The structure of HhDod<sup>B</sup> was solved by molecular replacement methods, using the atomic coordinates of HsDod<sup>A</sup> (Protein Data Bank code 2ccb) as a search model.

For detailed information see supplemental Experimental Procedures.

## RESULTS

**Structural Comparison of Dodecin from *H. salinarum* (HsDod<sup>A</sup>) and *H. halophila* (HhDod<sup>B</sup>)**—The crystal structure of dodecin from *H. salinarum* (HsDod<sup>A</sup>; superscript A for archaeal) revealed a highly symmetric, hollow-spherical shaped protein with an outer diameter of about 65 Å. The 7.4-kDa monomers of simple β1αβ2β3 topology are assembled into dodecamers composed of a β-sheet corpus with the α-helices exposed on the outside. Binding pockets for dimers of flavin and flavin-like ligands are located between the trimer substructures of the dodecameric assembly. Crystal structures of HsDod<sup>A</sup> with the ligands LCR, lumiflavin, RF, FMN, and FAD allowed the analysis of the dodecin-binding site in detail. HsDod<sup>A</sup> binds RF (*K<sub>D</sub>* of 36 nM) and the small ligand LCR (10 nM) with high affinity by using slightly different binding modes (13). When the ligand binding properties of a homologous protein from *Halorhodospira halophila* (HhDod<sup>B</sup>, superscript B for bacterial) were analyzed, the affinities for RF and LCR were found to be significantly lower (*K<sub>D</sub>* of 2.5 and 20.4 μM, respectively) as compared with HsDod<sup>A</sup>. To investigate the differences between the archaeal HsDod<sup>A</sup> and its bacterial HhDod<sup>B</sup> counterpart, the crystal structure of HhDod<sup>B</sup> was determined to a resolution of 2.6 Å (see supplemental Table 1).

In line with the overall 40% amino acid sequence identity, a structural comparison between the archaeal HsDod<sup>A</sup> and the bacterial HhDod<sup>B</sup> revealed a strong conservation of the dodecin monomer fold, with an overall root mean square deviation of 0.65 Å (59 C-α atoms), as well as the conservation of the dodecameric hollow spherical assembly (Fig. 2, A and B). However, despite their high similarity, the architecture of the flavin-binding site and the flavin-binding mode of HhDod<sup>B</sup> was strikingly different compared with HsDod<sup>A</sup>. Whereas HsDod<sup>A</sup> binds dimers of flavins with the *re*-sides of the isoalloxazine rings associated, HhDod<sup>B</sup> incorporated RF via *si-si* stacking (Fig. 2C).

As shown in Fig. 2D, the reduced size of the flavin-binding pocket due to the altered main chain conformation of the nearby β2 strand gives an explanation of the inverted binding mode of HhDod<sup>B</sup>. The backbone conformation of the Thr<sup>45</sup>–Ile<sup>49</sup> peptide stretch is not only caused by changes in the immediate HhDod<sup>B</sup> sequence. In the HhDod<sup>B</sup> structures, a phenylalanine side chain of a neighboring dodecin monomer (Phe<sup>40</sup>) wedges between β2 and the amphipathic helix, forming an edge-face interaction to a highly conserved aromatic residue (Trp<sup>57</sup>). The main chain shift narrows the binding pockets of

## Function of the Archaeal Dodecin

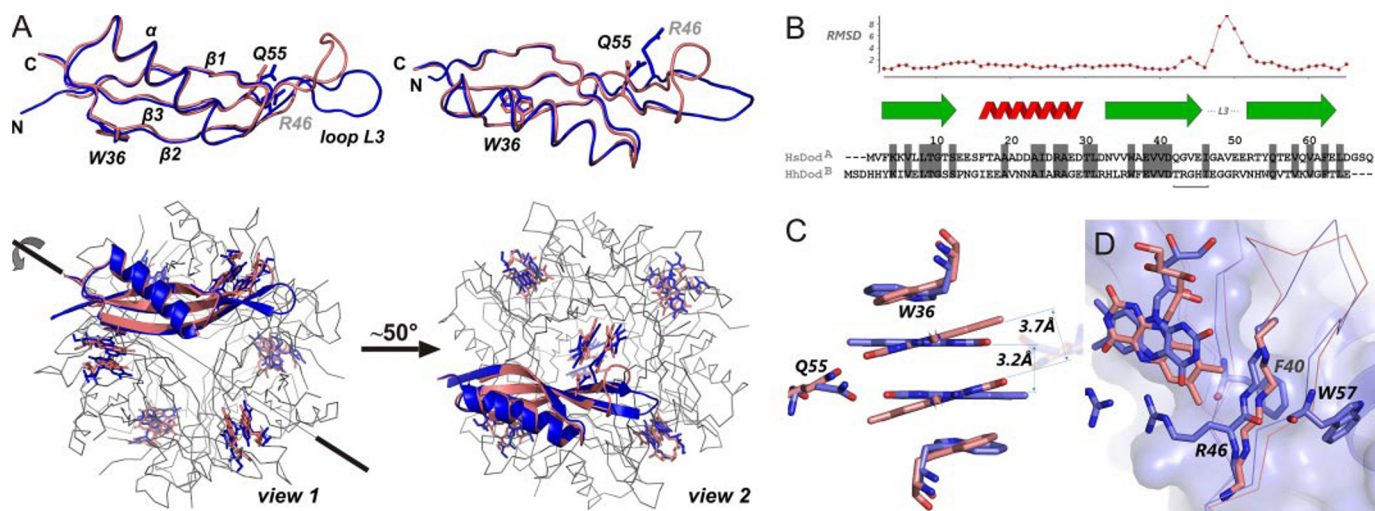


**FIGURE 2. Comparison of HsDod<sup>A</sup> and HhDod<sup>B</sup>.** *A*, superposition of the C- $\alpha$  traces of HsDod<sup>A</sup> (red) and HhDod<sup>B</sup> (blue) as separate monomers and as monomers part of the dodecameric assembly (superposition on the HsDod<sup>A</sup> C- $\alpha$  trace in gray with bound riboflavins in color code of monomers). *View 1* shows dodecin oriented along a 3-fold axis and *view 2* along a 2-fold axis. HsDod<sup>A</sup> labels are in black and HhDod<sup>B</sup> in gray. *B*, structure-based sequence alignment and C- $\alpha$  root mean square deviation between the archaeal HsDod<sup>A</sup> and the bacterial HhDod<sup>B</sup>. The largest structural deviations in C- $\alpha$  atoms between HsDod<sup>A</sup> and HhDod<sup>B</sup> involve residues 47–52 (50–55 of HhDod<sup>B</sup>). This peak corresponds to differences in the loop between the  $\beta 2$  and  $\beta 3$  strands. *C*, inverted binding of RF in HsDod<sup>A</sup> (red) and in HhDod<sup>B</sup> (blue). Trp<sup>36</sup> (W36) and Gln<sup>55</sup> (Q55), clamping and aligning the isoalloxazine rings in tetrad arrangements, are shown (HsDod<sup>A</sup> numbering). In contrast to HsDod<sup>A</sup>, the glutamine in HhDod<sup>B</sup> binds the flipped flavin of the dimer-related monomer. In both structures, the distance between the indole and the isoalloxazine aromatic rings is about 3.3 Å. *D*, deviation in the main chain architecture to meet the different requirements of ligand incorporation. The widened pocket of HsDod<sup>A</sup> allows accommodation of the dimethylated benzene ring in the *re-re* arranged aromatic tetrad (see minor peak in Fig. 2*B* between residues 42 and 46). Arg<sup>46</sup> (R46) of HhDod<sup>B</sup>, highly conserved in bacterial dodecins, accounts for hydrogen bonding to the isoalloxazine moiety. This isoalloxazine-protein interaction is missing in HsDod<sup>A</sup>. For clarity, side chains of HsDod<sup>A</sup> are omitted, and the binding pocket is reduced to the 2-fold related part.

HhDod<sup>B</sup> structure, promoting the tilted conformation of the *si-si*-stacked isoalloxazine moieties over the *re-re*-stacked conformation seen in the HsDod<sup>A</sup>.

Recently, FMN incorporation into the dodecin homolog from the bacterial thermophile *Thermus thermophilus* (TtDod<sup>B</sup>) was shown to be similar to RF binding to HhDod<sup>B</sup> (19). Mutation of arginine, corresponding to Arg<sup>46</sup> in HhDod<sup>B</sup>, forming H-bonds to the C-4=O and N-5 of the isoalloxazine, does not influence the mode of FMN binding. Supporting the impact of the main chain conformation of the  $\beta 2$ -strand, TtDod<sup>B</sup> narrows the binding pocket and forms edge-face interactions (Phe<sup>39</sup>/Tyr<sup>56</sup>), similarly as found in HhDod<sup>B</sup>.

**Light-induced Degradation of RF**—The light stability of free and dodecin-bound RF was determined by illuminating RF-dodecin complexes with light from a high pressure mercury lamp. Absorption spectra were recorded at various time points, and concentrations of RF and the degradation product LCR were monitored by fluorescence detection of chromatographically separated samples (Fig. 3*A* and supplemental Fig. 2, *A* and *B*). Similar to the free compound, HhDod<sup>B</sup>-bound RF decomposed into various fluorescent degradation products (see traces HhDod<sup>B</sup>\_ii and \_iii in Fig. 3*A*), but the half-life ( $t_{1/2}$ ) of 32 s for the unbound RF was 45-fold increased to 24.7 min in the bound state (Fig. 3*B*).

RF incorporated into HsDod<sup>A</sup> showed slightly lower stabilization as RF bound to HhDod<sup>B</sup> (RF/HhDod<sup>B</sup>) ( $t_{1/2}$  of 19.7 min) but in contrast was efficiently transformed into LCR. Even after 4 h of illumination, no other compound was detected at both wavelength couples (see traces HsDod<sup>A</sup>\_ii and \_iii in Fig. 3*A*). As depicted in Fig. 3*C*, 74% of the initial RF could be detected as either the LCR product (~67%) or intact RF (~7%). Free and dodecin-bound LCR did not show a change in absorption char-

acteristics during illumination, supporting that LCR is a rather stable end product of light-induced RF degradation (20).

**Spectroscopic Analysis of Free and Dodecin-bound RF**—To analyze the quenching competence of dodecin, time-resolved UV-visible spectroscopy was carried out using RF-reconstituted dodecins (RF/HsDod<sup>A</sup> and RF/HhDod<sup>B</sup>). The excited state dynamics of RF was recorded by exciting at three different spectral positions, inducing different electronic transitions, and providing different excess vibrational energies. Pulses centered at wavelengths of 476 nm ( $S_0/S_1$  transition), 388 nm ( $S_0/S_2$  transition, low energy wing), and 345 nm ( $S_0/S_2$  transition, high energy wing) were used to excite RF. Typical pulse energies were about 100 nJ. Probe pulses in the spectral range of 450–750 nm were generated in a sapphire crystal as single filament white light. Transient absorbance changes for the different pump wavelengths did not show any significant differences, which suggests that the  $S_2/S_1$  transition is faster than the time resolution of the experiment. Discussion of the time resolved data is thus restricted to the 388 nm excitation, yielding data with the best signal to noise ratio.

As illustrated by the transient absorbance changes seen in Fig. 4*A*, free and dodecin-bound RF showed entirely different spectral and dynamic characteristics. (*a*) While the excited state lifetime of free RF was longer than the maximum delay of the experiment (1.5 ns), bound RF displayed excited state lifetimes dramatically shortened to a few picoseconds. (*b*) The pattern of stimulated emission (SE, blue), ground state bleach (GB, blue) and excited state absorption (ESA, red) was strongly changed, as e.g. the extensive SE at 520–600 nm observed for free RF in aqueous solution was missing in both RF-dodecin complexes (21).

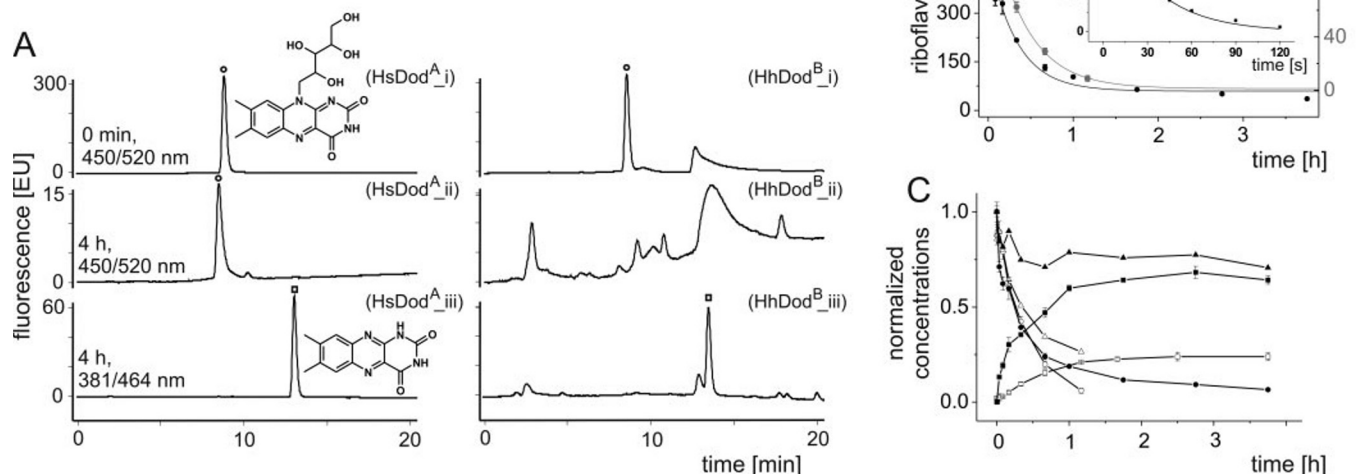


**FIGURE 3. Light-induced degradation of free and dodecin-bound RF.** A, illumination of free and dodecin-bound RF. Chromatographic profiles of RF/HsDod<sup>A</sup> (HsDod<sup>A</sup><sub>i</sub>-HsDod<sup>A</sup><sub>iii</sub>) and RF/HhDod<sup>B</sup> (HhDod<sup>B</sup><sub>i</sub>-HhDod<sup>B</sup><sub>iii</sub>) at 0 min and after 4 h of illumination with light. Fluorescence detection is performed at 520 (i, ii) and 464 nm (iii). Chemical structures for RF (○) and LCR (□) are shown as insets in fluorescence lanes. Note that the EU scale is different in lanes i–iii. B, molar concentrations of RF fitted to a first order decay; HsDod<sup>A</sup> (black circle, solid line) and HhDod<sup>B</sup> (gray circle, gray solid line) and free RF shown in inset. Half-lives were determined to be  $32 \pm 1.4$  s (free RF),  $1180 \pm 180$  s (19.7 min; HsDod<sup>A</sup>) and  $1480 \pm 230$  s (24.7 min, HhDod<sup>B</sup>), respectively. C, light stability of dodecin-bound RF (in air). Concentrations of RF and LCR incorporated into HsDod<sup>A</sup> (●/■) and HhDod<sup>B</sup> (○/□) and the respective overall concentrations (▲/△) are shown.

However, differences in spectra were also observed between RF bound to HsDod<sup>A</sup> and HhDod<sup>B</sup>. (a) The broad excited state absorption signal of RF/HsDod<sup>A</sup> did not extend into the long wavelength region, as seen for the bacterial RF/HhDod<sup>B</sup> as well as for free RF. (b) Excited state lifetimes of RF bound to HhDod<sup>B</sup> were slightly longer than of RF bound to HsDod<sup>A</sup>. Respective individual transients are shown in Fig. 4B.

**Flavin Concentrations during *H. salinarum* Growth**—Flavins were extracted from *H. salinarum* R1 (wild type) strain cells, chromatographically separated, and quantified by fluorescence. Recorded peak areas were correlated to the internal cell volume, calculated from the optical density of the cultures ( $OD_{578}$ ) at the respective day (Fig. 5A). The following strains and culture conditions were examined: *H. salinarum* wild type strain in the light (R1<sub>l</sub>) and in the dark (R1<sub>d</sub>), and a dodecin-deficient strain in the dark (R1Δdod<sub>d</sub>). Cells of the wild type strain, cultivated in the dark (R1<sub>d</sub>) as well as in the light (R1<sub>l</sub>), showed much higher FMN and FAD concentrations in the exponential growth phase (day 4 and 6) than in the stationary phase (Fig. 5B). In contrast, RF concentrations were low in the exponential and early stationary phase and high in the late stationary phase. RF regulation was most pronounced in R1<sub>d</sub> cells, where values reached  $18.2 \mu\text{M}$  in the late stationary phase (day 23).

In the deletion strain R1Δdod, FMN and FAD concentrations resembled levels of the wild type strain R1. However, a dramatic influence of the deleted dodecin could be seen in the concentrations of RF;  $18.6 \mu\text{M}$  in the wild type inoculation culture grown in the dark (R1<sub>d</sub>) is opposed by  $1.2 \mu\text{M}$  in the corresponding dodecin-deficient R1Δdod pre-culture (R1Δdod<sub>d</sub>). This difference was significantly decreased at day 4 but appeared again when the cultures ran into the late stationary phase (see also supplemental Table 2).

**LCR Concentrations during *H. salinarum* Growth**—In parallel to the quantitative analysis of flavins also the LCR cellular concentrations were determined during *H. salinarum* growth. As shown in Fig. 5C, concentrations at day 4 were low in cells of the wild type and the dodecin deletion strain. However, starting at day 6, LCR concentrations in the wild type cells cultured in light (R1<sub>l</sub>) were increased to about  $20 \mu\text{M}$ , whereas cells cultured in the dark (R1<sub>d</sub> and R1Δdod<sub>d</sub>) kept LCR molarities at low levels of  $5.4 \mu\text{M}$  at highest (R1<sub>d</sub>, day 35, see also supplemental Table 3).

**Ligand Analysis of Homologously Expressed HsDod<sup>A</sup>**—The strain R1dodHis<sup>+</sup> homologously expresses His-tagged dodecin. After extraction from the *H. salinarum* cytosol by a nickel-chelating resin, ligands bound to His-tagged dodecin *in vivo* were quantitatively determined by chromatographic separation and fluorescence detection. No FMN and FAD could be detected as natural ligands. As presented in Table 1, values for the RF cellular concentrations measured at the end of the exponential growth phase (day 7), in the middle (day 13), and the late stationary phase (day 21) correspond well to values of the *H. salinarum* wild type strain R1 (supplemental Table 3). Concentrations of dodecin-bound RF are in the range of the total cellular RF and suggest that in *H. salinarum* all RF is sequestered by dodecin.

**Expression of Dodecin during *H. salinarum* Growth**—Western blot analysis of *H. salinarum* cultures revealed that dodecin is regulated during growth. As seen in Fig. 6A, dodecin expression was generally induced upon transition into the exponential growth phase, irrespective of the presence of light. After induction of dodecin expression, the protein level varied slightly under both conditions. The copy number of dodecin in an R1<sub>d</sub> culture at the stationary phase was determined to 8000, corresponding to a concentration of  $9.2 \mu\text{M}$  (see supplemental Fig.

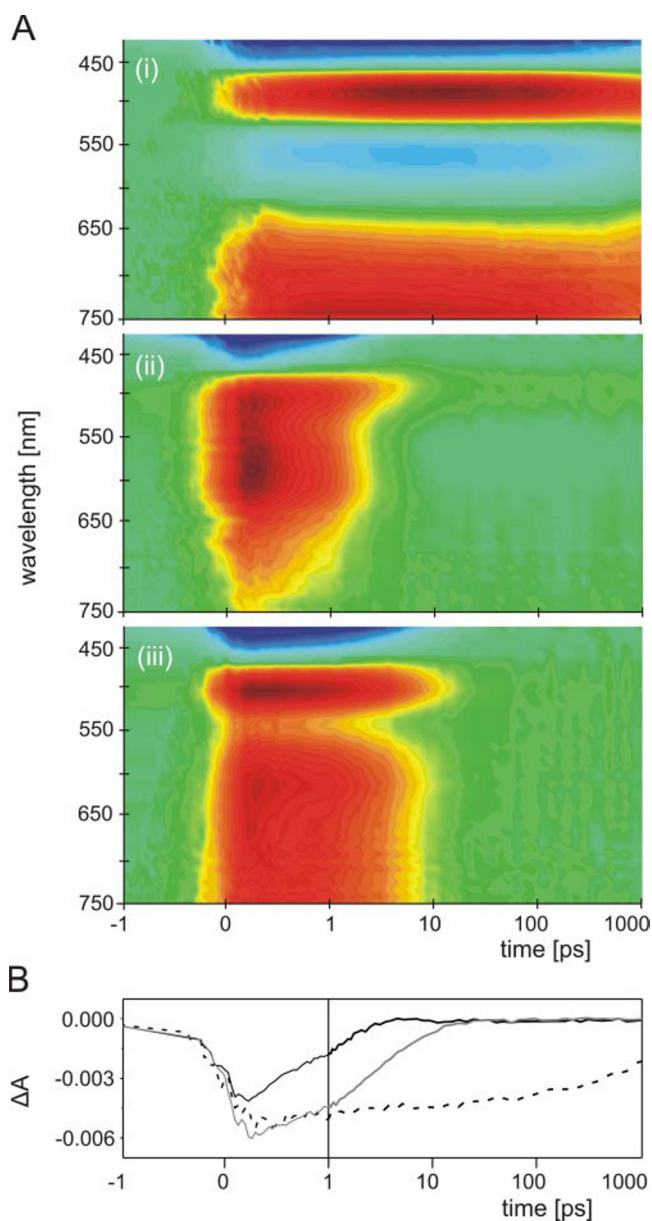


FIGURE 4. Time-resolved spectroscopic characterization of free and dodecin-bound RF. *A*, excitation of RF (panel *i*), RF incorporated in HsDod<sup>A</sup> (RF/HsDod<sup>A</sup>) (panel *ii*), and in HhDod<sup>B</sup> (RF/HhDod<sup>B</sup>) (panel *iii*) performed at 388 nm with sapphire white light as the probing pulse. Positive absorbance changes are shown in red and negative in blue. *B*, transient absorbance changes at 451 nm. Free RF is shown as a dashed line in black, the corresponding RF/HsDod<sup>A</sup> and RF/HhDod<sup>B</sup> complexes in black and gray solid lines, respectively.

4A). RT-PCR was employed to quantitatively monitor the regulation of dodecin at the mRNA level during the time period of the relatively constant dodecin expression. The mRNA levels at day *i* ( $\Delta Ct_i$ ) were related to the starting level at day 4 ( $\Delta Ct_{x1}$ ). Increasing values indicate that dodecin was slightly up-regulated at the transcriptional level during growth (Fig. 6B). Comparison of dodecin mRNA levels in cells grown in light ( $\Delta Ct_l$ ) and in the dark ( $\Delta Ct_d$ ) revealed that dodecin was not regulated by light at the transcriptional level. For a discussion of the outlying dodecin mRNA levels at day 9, see supplemental Experimental Procedures and supplemental Fig. 4B.

*LCR Concentrations under Laboratory Conditions and in the Native Environment*—Table 2 lists the LCR concentration in non-inoculated fresh medium, either stored in light or in dark for several weeks, and in waters taken from hypersaline ponds, an environment where Haloarchaea occur in high numbers. Whereas in the *H. salinarum* growth medium LCR was found to be present in high nano- to low micromolar amounts, the concentration of LCR in the natural environment was  $10^2$ – $10^3$ -fold lower.

## DISCUSSION

*Dodecin Buffers the Flavin Concentration during H. salinarum Growth*—The analysis of the flavin metabolism revealed that cellular RF concentrations were significantly dependent on dodecin. As illustrated in Fig. 5B, the RF level was 4–16-fold higher in *H. salinarum* wild type cells (R1\_d) as compared with the dodecin-deficient strain (R1 $\Delta$ dod\_d), indicating the influence of dodecin. The nature of dodecin as a rigid, dodecameric RF-binding particle does not suggest a direct regulative role in flavin biosynthesis. The increased RF concentrations in wild type cells most likely occur from indirectly influencing the flavin metabolism by depleting the cytosol of RF and suppressing a down-regulation of flavin synthesis (22–24). Data from RF extractions of the dodecin overexpression strain R1dodHis<sup>+</sup>, which demonstrated that the all cellular RF can be sequestered by dodecin, are in line with the assumption that the impact of dodecin on the flavin biosynthesis results from its capacity to store RF (see Table 1).

The benefit of creating a reservoir of RF is connected to the expression profile of dodecin and is illustrated in Fig. 7A. Induced during exponential growth (stage 1), dodecin is constitutively expressed and stores RF, increasing in concentration during the stationary phase (stage 2). If the environment changes toward favorable growth conditions, simulated by re-inoculation into rich culture media, dodecin is down-regulated (see Fig. 6A), and the collected RF subsequently becomes available for the synthesis of FMN and FAD (stage 3). This regulation of dodecin enables a fast response of *H. salinarum* to changing environmental conditions.

*Working Mode 1, Ultrafast Quenching of Excited RF*—X-ray structural investigations revealed that the isoalloxazine of bound RF is deeply buried in the protein interior (see Fig. 2D). The loop L3, connecting HsDod<sup>A</sup> strands  $\beta 2$  and  $\beta 3$ , represents the most flexible part of the structure and has been proposed to seal the binding pocket and shield the isoalloxazine ring from the environment (13). Although protection of the isoalloxazine substructure from chemical activation can easily be achieved by steric restrictions, the protection from light-induced reactions is more demanding.

The key step in flavin photochemistry is the photoexcitation of the isoalloxazine electronic system into an excited singlet state, which is generally accompanied by a subsequent intersystem crossing into the triplet state. Excited singlet and triplet state energies can be released in intra- and intermolecular reactions, constituting the flavin photochemistry. Although unable to inhibit the initial step of the photoinduced formation of the excited state, proteins can efficiently suppress light-induced reactivity. As has been shown for the chicken RfBP, binding

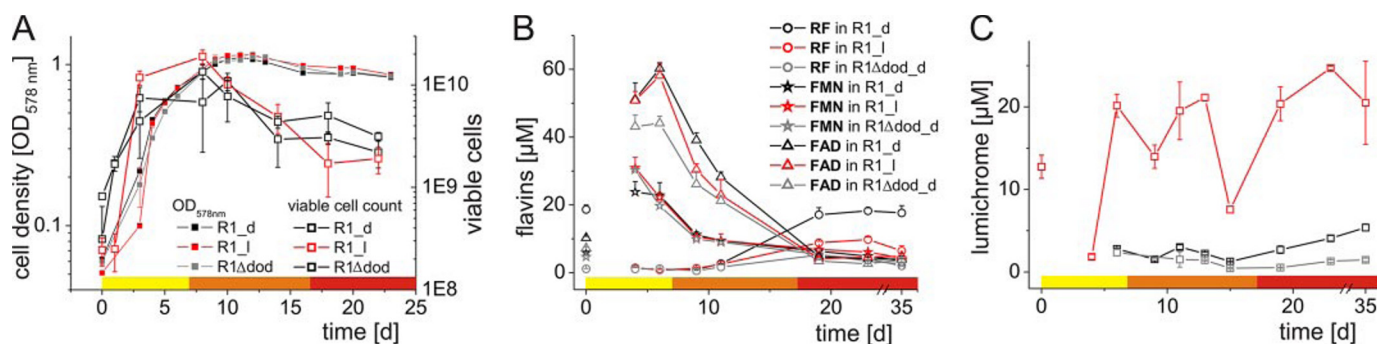


FIGURE 5. **Flavin and LCR concentrations during *H. salinarum* growth.** *A*, growth curves of *H. salinarum* strains R1 (wild type) and R1Δdod (dodecin deleted). The color code of growth phases (exponential, yellow; early stationary, orange; late stationary, red) is used in *B* and *C*, and Fig. 7*A*. *B*, flavin concentrations during *H. salinarum* growth. Quantitative analysis of intracellular flavin reveals similar FMN (star) and FAD (Δ) concentrations in wild type cells cultured in the dark (R1<sub>d</sub>, black) and in the light (R1<sub>l</sub>, red), as well as in the deletion strain R1Δdod in the dark (R1Δdod<sub>d</sub>, gray). Concentrations of RF (○) show major differences with respect to light and dodecin. *C*, LCR concentrations during *H. salinarum* growth. LCR molar concentrations are about 10-fold increased in the *H. salinarum* wild type strain R1 grown in light (R1<sub>l</sub>, red) as compared with cells grown in the dark (R1<sub>d</sub>, black) or depleted in dodecin (R1Δdod<sub>d</sub>, gray). LCR concentrations were below the detection limit (<0.5 μM) in the R1Δdod<sub>d</sub> inoculation culture and at day 4 in cultures R1<sub>d</sub> and R1Δdod<sub>d</sub>.

**TABLE 1**  
RF concentrations in cultures of R1dodHis<sup>+</sup>

Day	Dark		Light	
	Bound RF	Total RF	Bound RF	Total RF
	μM			
7	0.88 ± 0.12	1.50 ± 0.03	1.16 ± 0.05	1.11 ± 0.11
13	1.89 ± 0.05	1.57 ± 0.15	1.34 ± 0.27	1.16 ± 0.12
21 <sup>a</sup>	17.98 ± 1.25	19.38 ± 1.11	8.06 ± 0.91	11.57 ± 0.72

<sup>a</sup> Values were generated in an individual experiment.

**TABLE 2**  
LCR concentrations in *H. salinarum* media and in the natural habitat

	Fresh medium <sup>a</sup>		Old medium <sup>b</sup>		Natural habitat <sup>c,d</sup>	
	Dark	Light	Dark	Light	Sample 1	Sample 2
	μM					
LCR	0.3 ± 0.02	2.1 ± 0.01	1.58 ± 0.1	0.17 ± 0.01	0.011	0.0034

<sup>a</sup> Freshly prepared media were kept for 2 days in the dark or in the light.

<sup>b</sup> Media of *H. salinarum* cultures were grown to the late stationary phase.

<sup>c</sup> Extraction of two independent water samples were from the solar salterns in Eilat, Israel.

<sup>d</sup> Values were determined by standard addition method.

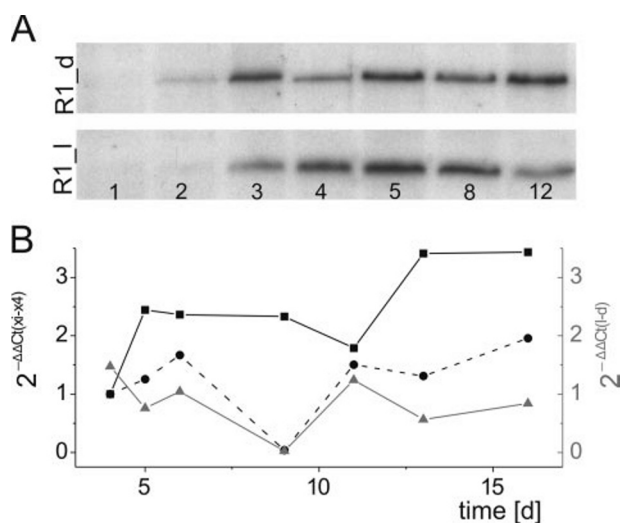


FIGURE 6. **Dodecin protein and mRNA levels during growth of *H. salinarum*.** *A*, Western blot analysis of dodecin in R1 wild type strain grown in the dark (R1<sub>d</sub>) and in light (R1<sub>l</sub>). *B*, analysis of the dodecin mRNA levels in cells of R1<sub>d</sub> (■), R1<sub>l</sub> (●, dashed line), and R1Δdod<sub>d</sub> (gray triangle) in the time period of the rather constant dodecin expression observed in *A*. A  $2^{-\Delta\Delta Ct(x_i-x_4)}$  value of 1 means no difference in the dodecin mRNA level at the respective day compared with reference day 4;  $1/2$  and 2, a 2-fold down-regulation and up-regulation, respectively.  $2^{-\Delta\Delta Ct(l-d)}$  values illustrate the differences in dodecin mRNA levels when cells grown in light (R1<sub>l</sub>) and in dark (R1<sub>d</sub>).

pockets, clamping the isoalloxazine ring between aromatic moieties, can strongly modify RF photochemistry by efficiently shortening the lifetime of the RF excited state (11, 25). Herein, the indole moiety of the tryptophan, holding the isoalloxazine ring of RF, quenches the excited state lifetime by the ultrafast transfer of electrons onto the excited flavin, creating a short-lived RF/tryptophan radical pair.

Time-resolved spectroscopy performed on the dodecins RF/HsDod<sup>A</sup> and RF/HhDod<sup>B</sup> recorded ground state recovery within a few picoseconds, and thus demonstrates a similarly efficient depopulation of RF excited states as reported for chicken RfBP. Based on the similar architecture of the chicken RfBP and the dodecin binding pockets, we suggest also that in the dodecins HsDod<sup>A</sup> and HhDod<sup>B</sup> the indole moieties of the adjacent tryptophans transfer the electron for RF quenching. Considering the tryptophan-isoalloxazine distances of 3.3 Å in the HsDod<sup>A</sup> and the HhDod<sup>B</sup> binding pockets, which are shorter than the respective distances of tryptophan (Trp<sup>156</sup>)-isoalloxazine (3.7 Å) and tyrosine (Tyr<sup>75</sup>)-isoalloxazine (3.7 Å) in the chicken RfBP, electron transfer can be estimated to take place within the sub-picosecond time scale (26, 27).

It has to be mentioned that the current view on the dodecin quenching characteristic is based on the extrapolation from similar proteins. At present, it can just be speculated to which extent electronic interactions between the stacked RF dimers increase the complexity of the photochemical behavior.

**Working Mode 2, Directed Degradation of Excited RF**—When incorporated into HsDod<sup>A</sup>, we found that RF was protected from fast degradation but also from unspecific decomposition. Whereas the enhanced stability of RF is the result of the ultrafast recovery of the RF ground state, the almost quantitative transition of RF to LCR could be recognized as the key characteristic of an alternative working mode coupled to RF storage. As this directed degradation is coordinated with the high affinity of dodecin for LCR, HsDod<sup>A</sup> allows an overall compartmentalized reaction, which is neutral to the cellular environment, and establishes an alternative pipeline for the depopulation of

## Function of the Archaeal Dodecin

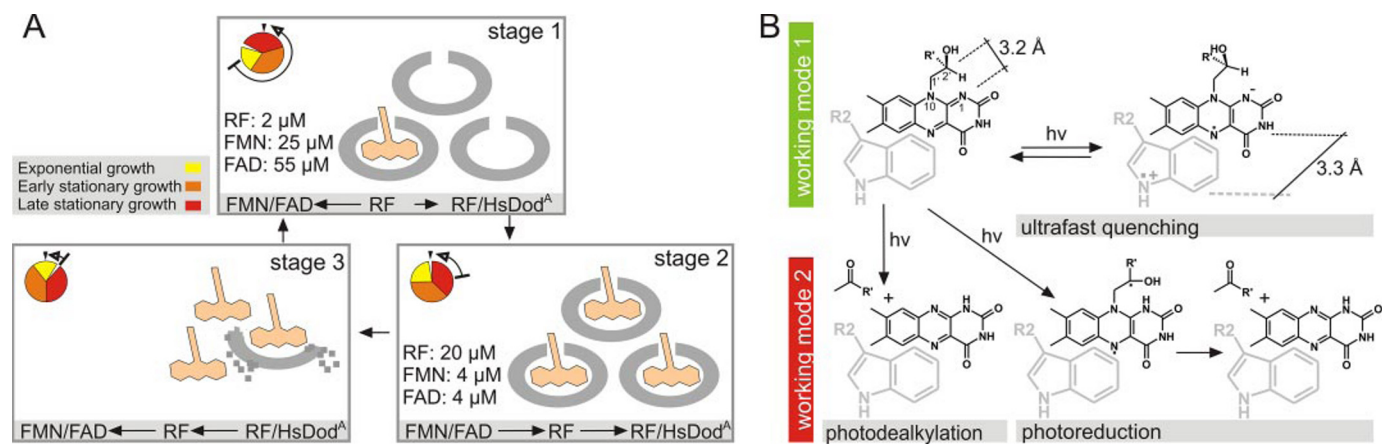


**FIGURE 7. Working scheme of the archaeal dodecin on the cellular and on the protein level.** *A*, dodecin cycle. Dodecin expression is induced in the exponential phase. Although present, the uptake of FMN and FAD is prevented by their low affinity (*stage 1*). In the stationary phase, RF (orange) from degradation of flavins and/or biosynthesis is sequestered by dodecin, establishing a flavin buffer (*stage 2*). Stored RF is available for biosynthesis of FMN and FAD when favorable condition induced metabolic activity (early exponential growth phase, *stage 3*). Intracellular flavin concentrations are given in insets. Attached schemes abstract the interplay of free RF, bound RF (RF/HsDod<sup>A</sup>), and converted RF (FMN/FAD). *B*, working modes of HsDod<sup>A</sup>. Shown is a model for the nondestructive quenching (working mode 1, green) and the destructive dealkylation reaction (working mode 2, red) as parallel reactions. Photoreduction and photodealkylation are reported to lead to LCR as a degradation product. Because of the high affinity of HsDod<sup>A</sup> for LCR, LCR is kept captured in the binding pocket. The intermediate state in working mode 1 is shown as a charged radical pair prior to a putative protonation/deprotonation step.

RF excited states. A rationale for installing a destructive dealkylation of RF as a second reaction might be the possibility to prevent unspecific reactivity of RF, leading to reactive (degradation) species that could not be controlled by protein ligand binding. The alternative working mode constitutes an emergency pathway for relaxation of light-activated RF, which might be of particular relevance for Haloarchaea that generally occur in bright light environments. Recently, directed flavin degradation was also reported for the FMN-binding protein BluB from *Sinorhizobium meliloti*. In contrast to dodecin, which sacrifices RF for the cellular integrity, BluB degrades FMN to deliver a cobalamin building block (28, 29).

**Reaction Control in Dodecins**—As illustrated in Fig. 7*B*, non-invasive ultrafast quenching of RF excited states and destructive dealkylation are considered as parallel reactions downstream of the excited RF. Ultrafast quenching is the primary process and is responsible for the increased lifetime of dodecin-bound RF.

The high selectivity of the degradation reaction is likely supported by the extensive decrease in RF excited state lifetime, as only reactions that proceed within the narrow time window of picoseconds can compete with ultrafast quenching. Such competing ultrafast processes require a reaction partner in close proximity that is fulfilled for the intramolecular reaction mode. Mechanistically, the strictly intramolecular photodealkylation and the intramolecular mode of photoreduction can be envisioned as routes to lumichrome. Both reactions were reported to proceed from the excited singlet state, and thus in the time range of the excited state lifetime of dodecin-bound RF (4). Moreover, both pathways pass a six-membered cyclic transition state that is pre-organized in RF bound to HsDod<sup>A</sup> (N1-C10a-N10-C1'-C2'-H2') and could well represent the structural base for the selection of RF dealkylation (4, 30–32). This view is supported by the even higher selectivity of RF dealkylation in the E45A mutated dodecin (HsDod<sup>A,E45A</sup>). The lack of Glu<sup>45</sup> mediated ribityl chain bonding, and the enhanced conformational flexibility might allow fine-tuning the geometry of

the transition state. For a short description of RF binding in HsDod<sup>A,E45A</sup> and the degradation of RF bound to HsDod<sup>A,E45A</sup> see the supplemental material. The coordination of the ribityl chain influences the degradation spectrum (see supplemental text and supplemental Fig. 5, *A* and *B*).

As illustrated in Fig. 4*A*, transient absorption changes recorded for RF/HsDod<sup>A</sup> and RF/HhDod<sup>B</sup> revealed significant differences in the electronic landscapes of the respective RFs. In particular, the recovery of the RF ground state, critical for suppressing the RF light-induced reactivity, was faster for the archaeal dodecin. A satisfactory global fit analysis of the two data sets obtains two time constants similar for both proteins (HsDod<sup>A</sup>, 0.9 and 6.6 ps; HhDod<sup>B</sup>, 2 and 9.8 ps). The individual weights and the spectral characteristics in the corresponding amplitude spectra are, however, clearly different, indicating different reaction channels for excited state quenching in the archaeal and the bacterial dodecin.

It cannot be stated that the spectral behavior is the only determinant of the unspecific photodegradation of RF bound to HhDod<sup>B</sup>. Considering the low affinity of HhDod<sup>B</sup> for RF ( $K_D$  2.5  $\mu\text{M}$  versus 36 nM for RF/HsDod<sup>A</sup>), a decomposition of RF in the unbound state of a dynamic binding rebinding process cannot be ruled out.

**Dodecin Working Mode 2 Leads to the Accumulation of LCR**—Although the catalytic properties of flavins are widely used, only a few examples of the physiological importance of LCR have been reported (33, 34). Instead, LCR is known as a toxic substance, transferring light energy to substrates (photosensitization type 1) and oxygen (photosensitization type 2), creating reactive compounds like singlet state oxygen (35). Accordingly, we found a sharp decrease of cell density when *H. salinarum* was grown in the light and in the presence of 40  $\mu\text{M}$  LCR. In the dark, LCR did not effect cell growth (see supplemental Fig. 3*B*).

In our experiments on *H. salinarum* cells grown under laboratory-rich conditions, we found intracellular concentrations of LCR in the low micromolar range, even when cells were

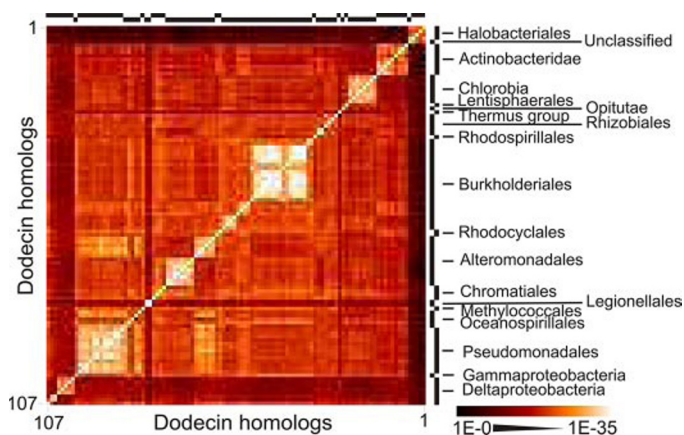


FIGURE 8. **Rampp plot of dodecin homologous sequences.** 107 sequences identified as homologs of HsDod<sup>A</sup> are listed according to standard taxonomy of the respective species and blasted against each other. *E*-values are arranged in a two-dimensional matrix with colors representing the conservation according to the legend at left. Each pixel represents the *E*-value of the sequence pair at the respective *horizontal* and *vertical* axis. The archaeal subfamily clusters as a highly homologous group of sequences, with significantly lower similarity to bacterial dodecins. This is indicated by a dark frame with a bright spot along the diagonal (for a list of organism see supplemental Fig. 6 and Fig. 7).

grown in the dark where light-induced degradation of RF was prevented. Analysis of non-inoculated *H. salinarum* growth medium revealed LCR concentrations of 0.3  $\mu\text{M}$  in fresh and 2.1  $\mu\text{M}$  in light-incubated medium (see Table 2), suggesting that the high levels of internal LCR are the result of the amphiphilic nature of LCR, which allows this compound to enter the cell interior via passive diffusion across the cell membrane. A concentration of 200  $\mu\text{M}$ , as reported for LCR in seawater (36), and concentrations of 2 and 10 nM, as recorded in samples from the natural environment (see Table 2), imply that different from laboratory conditions *H. salinarum* is not exposed to high exogenous levels of LCR under native conditions. The LCR binding capacity of dodecin can therefore rather be regarded as a functional element that acts to keep LCR sequestered, generated by the dodecin working mode.

While reflecting non-native conditions, tracing the LCR concentrations under laboratory conditions illustrates how *H. salinarum* deals with the accumulation of LCR. Even non-physiologically high internal levels of 12.8  $\mu\text{M}$ , as detected in the R1 inoculation culture, were decreased within a few days to concentrations lower than 0.5  $\mu\text{M}$  (day 4 in dark; 1.8  $\mu\text{M}$  in light). This seems to be achieved by releasing LCR during down-regulation of dodecin in early exponential growth and the dilution of the diffusible LCR to the concentration level of the habitat. Temporarily enhanced LCR concentrations might thereby be tolerated in cells undergoing high metabolic activity.

**Dodecins in Archaea Versus Dodecins in Bacteria**—As shown in Fig. 8, protein alignments reveal that dodecins cluster in an archaeal and bacterial subgroup. Whereas widely distributed within bacteria, archaeal dodecins are only found in the phylum Haloarchaea (see also supplemental Figs. 6 and 7). We initially assumed that the haloarchaeal dodecin clade reflects the adaptation of these species to hypersaline conditions (37). However, as reported here, the structural analysis of HsDod<sup>A</sup> and HhDod<sup>B</sup> revealed that the archaeal and the bacterial species

have a different architecture of their RF-binding sites. Biophysical analyses also indicated fundamentally different spectroscopic properties, and light degradation experiments showed entirely different degradation spectra (see Figs. 3 and 4). Although our data clearly suggest that the function of the archaeal dodecin is to store RF, the role of the bacterial dodecin is not clear at present. The structurally and functionally characterized bacterial dodecins from *H. halophila* (HhDod<sup>B</sup>) and *T. thermophilus* (TtDod<sup>B</sup>) show binding spectra different from that of *H. salinarum* (HsDod<sup>A</sup>), supporting the flavins FMN and FAD in a functional role (13, 19). Recently, the crystal structure of the NADH:FMN oxidoreductase (EmoB) has been published, revealing FMN dimers bound as *si-si*-stacked dimers, similar as found in the bacterial dodecins (38). However, whereas dodecin provides two identical binding positions deeply buried in the protein interior, EmoB binds the FMN molecules of a stacked dimer differently and exposed at the protein surface, promoting a *ping-pong* mechanism in catalysis. For a more detailed view on a putative function of the bacterial dodecin see supplemental text and supplemental Fig. 8.

**Concluding Remarks**—We have shown that RF storage for fast delivery of FMN and FAD is not restricted to higher organisms but also operates in prokaryotes. The function of HsDod<sup>A</sup> is to sequester RF under growth limitation and to release this compound into the biosynthesis of FMN and FAD, when the metabolic activity is induced by favorable conditions, thus maintaining an elevated level of flavin throughout the *H. salinarum* life cycle. Because of the high reactivity of flavins, storage of RF bears a risk for the cellular integrity. To prevent uncontrolled reactions with potent molecules, HsDod<sup>A</sup> binds RF with high affinity and encapsulates the isoalloxazine rings at the bottom of binding pockets that are sealed with flexible loops. Protection from light-induced reactivity is achieved by ultrafast quenching of RF excited state lifetimes, putatively by a similar pathway as has been described for eukaryotic RfBPs. Quenching is assisted by an emergency relaxation of dealkylating the excited RF to LCR. By coordinating this directed degradation with the affinity for LCR, the reaction proceeds in the nanospace of the HsDod<sup>A</sup> binding pocket and is neutral to the cellular environment.

**Acknowledgments**—We are very grateful to Ursel Grampp-Heider, Evy Sauer, Gabor Meser, and Oliver Schmidt for assistance in the laboratory; Marko Rampp for support in bioinformatics on dodecin; Georg Lentzen (Bitop, Germany) for providing ectoin; Frank Siedler for the set-up of high pressure liquid chromatography with fluorescence detection; Jerry Eichler and Aharon Oren for samples from the solar salterns of the Israel Salt Co. (Eilat, Israel); Lissy Weyher-Stingl for analysis of dodecins by mass spectrometry; Ehmke Pohl and Clemens Schulze-Briese (SLS, Zurich, Switzerland); and Joanne McCarthy and Didier Nurizzo (ESRF, Grenoble, France) for beamline support. We also thank Mike Dyall-Smith, Luis Moroder, Alfons Penzkofer and Petra Wollmann for reading and discussing the manuscript.

## REFERENCES

- Barquera, B., Zhou, W., Morgan, J. E., and Gennis, R. B. (2002) *Proc. Natl. Acad. Sci. U. S. A.* **99**, 10322–10324

## Function of the Archaeal Dodecin

- Massey, V. (2000) *Biochem. Soc. Trans.* **28**, 283–296
- Müller, F. (ed) (1991) *Chemistry and Biochemistry of Flavoenzymes*, Vol. 1, pp. 1–71, CRC Press, Boca Raton, FL
- Heelis, P. F. (1991) in *Chemistry and Biochemistry of Flavoenzymes* (Müller, F., ed) Vol. 1, pp. 171–193, CRC Press, Boca Raton, FL
- Sazanov, L. A., and Hinchliffe, P. (2006) *Science* **311**, 1430–1436
- Aubert, C., Vos, M. H., Mathis, P., Eker, A. P., and Brettel, K. (2000) *Nature* **405**, 586–590
- Mees, A., Klar, T., Gnau, P., Hennecke, U., Eker, A. P. M., Carell, T., and Essen, L.-O. (2004) *Science* **306**, 1789–1793
- Crosson, S., and Moffat, K. (2002) *Plant Cell* **14**, 1067–1075
- Monaco, H. L. (1997) *EMBO J.* **16**, 1475–1483
- Foraker, A. B., Khantwal, C. M., and Swaan, P. W. (2003) *Adv. Drug Delivery Rev.* **55**, 1467–1483
- Mataga, N., Chosrowjan, H., Shibata, Y., Tanaka, F., Nishina, Y., and Shiga, K. (2000) *J. Phys. Chem.* **104**, 10667–10677
- Bieger, B., Essen, L. O., and Oesterhelt, D. (2003) *Structure (Lond.)* **11**, 375–385
- Grininger, M., Zeth, K., and Oesterhelt, D. (2006) *J. Mol. Biol.* **357**, 842–857
- Grininger, M., Seiler, F., Zeth, K., and Oesterhelt, D. (2006) *J. Mol. Biol.* **364**, 561–566
- Koch, M. K., and Oesterhelt, D. (2005) *Mol. Microbiol.* **55**, 1681–1694
- Marg, B.-L., Schweimer, K., Sticht, H., and Oesterhelt, D. (2005) *Biochemistry* **44**, 29–39
- Huber, R., Koehler, T., Lenz, M. O., Bamberg, E., Kalmbach, R., Engelhard, M., and Wachtveitl, J. (2005) *Biochemistry* **44**, 1800–1806
- Twilmeyer, J., Wende, A., Wolfertz, J., Pfeiffer, F., Panhuysen, M., Zaigler, A., Soppa, J., Welzl, G., and Oesterhelt, D. (2007) *PLoS One* **2**, e1064
- Meissner, B., Schleicher, E., Weber, S., and Essen, L.-O. (2007) *J. Biol. Chem.* **282**, 33142–33154
- Holzer, W., Shirdel, J., Zirak, P., Penzkofer, A., Hegemann, P., Deutzmann, R., and Hochmuth, E. (2004) *Chem. Phys.* **308**, 69–78
- MacFarlane, A. W. I. V., and Stanley, R. J. (2001) *Biochemistry* **40**, 15203–15214
- Winkler, W. C., Cohen-Chalamish, S., and Breaker, R. R. (2002) *Proc. Natl. Acad. Sci. U. S. A.* **99**, 15908–15913
- Gerhardt, S., Haase, I., Steinbacher, S., Kaiser, J. T., Cushman, M., Bacher, A., Huber, R., and Fischer, M. (2002) *J. Mol. Biol.* **318**, 1317–1329
- Vitreschak, A. G., Rodionov, D. A., Mironov, A. A., and Gelfand, M. S. (2002) *Nucleic Acids Res.* **30**, 3141–3151
- Zhong, D., and Zewail, A. H. (2001) *Proc. Natl. Acad. Sci. U. S. A.* **98**, 11867–11872
- Tanaka, F., Chosrowjan, H., Taniguchi, S., Mataga, N., Sato, K., Nishina, Y., and Shiga, K. (2007) *J. Phys. Chem.* **111**, 5694–5699
- Page, C. C., Moser, C. C., Chen, X., and Dutton, P. L. (1999) *Nature* **402**, 47–52
- Gray, M. J., and Escalante-Semerena, J. C. (2007) *Proc. Natl. Acad. Sci. U. S. A.* **104**, 2921–2926
- Taga, M. E., Larsen, N. A., Howard-Jones, A. R., Walsh, C. T., and Walker, G. C. (2007) *Nature* **446**, 449–453
- Moore, W. M., Spence, J. T., Raymond, F. A., and Colson, S. D. (1963) *J. Am. Chem. Soc.* **85**, 3367–3372
- Walker, W. H., Hemmerich, P., and Massey, V. (1970) *Eur. J. Biochem.* **13**, 258–266
- Hemmerich, P. (1976) *Fortschr. Chem. Org. Naturst.* **33**, 451–527
- Ueno, K., and Natori, S. (1987) *J. Biol. Chem.* **262**, 12780–12784
- Tsukamoto, S., Kato, H., Hirota, H., and Fusetani, N. (1999) *Eur. J. Biochem.* **264**, 785–789
- Sikorski, M., Sikorska, E., Koziolowa, A., Gonzalez Moreno, R., Bourdelande, J. L., Steer, R. P., and Wilkinson, F. (2001) *J. Photochem. Photobiol. B Biol.* **60**, 114–119
- Scarano, G., and Morelli, E. (1994) *Anal. Chim. Acta* **296**, 277–284
- Madern, D., Ebel, C., and Zaccai, G. (2000) *Extremophiles* **4**, 91–98
- Nissen, M. S., Youn, B., Knowles, B. D., Ballinger, J. W., Jun, S.-Y., Belchik, S. M., Xun, L., and Kang, C. (2008) *J. Biol. Chem.* **282**, 28710–28720